GRANULAR PRESSURE MEASUREMENT IN FLUIDIZED BEDS

S. Kumar, D. P. Hart, and C. E. Brennen
California Institute of Technology
Pasadena, California

Abstract

Experiments were carried out to measure the additional pressure, called the granular pressure, which is exerted on the containing wall of a fluidized bed due to particle collisions with that wall. Measurements were made for water fluidized beds using glass beads of 1.3 mm and 3 mm diameter, lead shot of 2.1 mm diameter and plastic particles. The granular pressure was observed to increase to a maximum and then decrease to zero as the solid fraction of the bed was reduced. The magnitude of the granular pressure was much larger than the values expected on the basis of previous experiments.

1. Introduction

The objective of this experiment was to measure the granular pressure in solid–liquid flows, specifically in fluidized beds. The granular pressure is defined as the pressure exerted on the containing walls due to the collisions of particles with those walls; the total pressure is the sum of the granular pressure and the fluid pressure. Collision statistics were obtained by measuring the distribution of collision impulses on a flush mounted transducer and converting these to granular pressures.

2. Notation

A	active surface area of the hydrophone
d	particle diameter
f	force exerted on active area of the hydrophone
$F(v^*)$	cumulative collision impulse probability function
h	manometer reading
H	distance between manometer taps in the fluidized bed
I	impulse
J_{f_s}	drift flux
k	constant in hydrophone calibration
m	mass of the particle
P	granular pressure
Re	Reynolds number based on terminal velocity = $\rho_f d u_\infty / \mu_f$
Re_f	Reynolds number based on fluid velocity= $\rho_f d u_f / \mu_f$
u	impact velocity of the particle
$\overline{u}$	mean impact velocity of the particle
$\overline{u^2}$	mean square impact velocity of the particle
u_f	mean fluid velocity in fluidized bed
u_∞	terminal velocity of single particle
v	peak voltage output level
v^*	threshold voltage level
v'	maximum noise voltage level
$\phi(v)$	collision impulse probability density function
μ_f	viscosity of the fluid
ν	solid fraction of the fluidized bed
ρ_f	density of the fluid
ρ_s	density of the solid particle

3. Experimental Facility

The experiments employed a water fluidized bed in a 10.2 cm diameter lucite tube using several different types of particles, as described in Table 1. The fluidized bed, which is a part of closed loop flow system, is shown schematically in Figure 1. A flow straightener eliminates any swirl and reduces nonuniformity in the flow prior to entering the bed. Carlos and Richardson (1968) noted that the magnitude of the unsteady motion in a fluidized bed is very sensitive to imperfections in the inflow. They went to considerable lengths to eliminate such imperfections by installing special flow smoothing devices just below screen at the bottom of the bed. In the present case a honeycomb flow straightner followed by a 29.2 cm high bed of 3.0 mm dia particles was installed at the bottom of the bed.

Points A and B are connected to a water manometer which measures the pressure drop in the fluidized bed. The flow rate through the bed is measured using a calibrated electromagnetic flow meter and is varied by means of a throttle valve. The hydrophone which is used to measure wall collisions is flush mounted in the fluidized bed at the location shown in Figure 1, 43 cm or 4.2 pipe diameters from the injection screen. The solid

fraction, ν, of the bed is deduced from the bed height, h, since νh must be constant; the constant was evaluated by experimentally measuring the maximum solid fraction at the minimum bed height. The solid fraction could also be calculated from the manometer reading. If H is the distance between points A and B and h is the difference in manometer levels, then in the absence of frictional effects, the solid fraction is given by

$$\nu = \frac{h}{H(\rho_s/\rho_f - 1)} \tag{2}$$

Table 1: Particles and Associated Data

Material	Shape	Diameter d(mm)	Specific Gravity, ρ_s	Terminal Velocity (cm/s)	Re, $\rho_f u_\infty d/\mu_f$
Glass	Spherical	1.3	2.5	19.3	250
Glass	Spherical	3.0	2.5	31.8	954
Lead	Spherical	2.1	11.4	83.2	1748
PVC	Cylindrical	(a)	1.43	16.0	440

(a): diameter of 2.75 mm and length of 3.5 mm

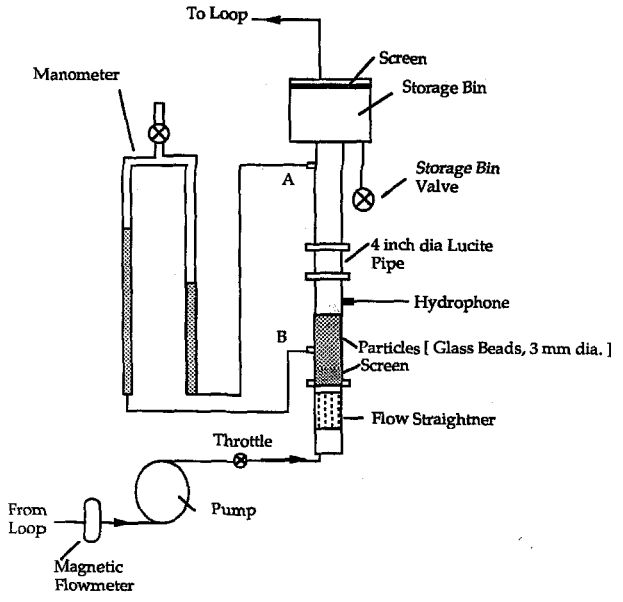

Figure 1: Schematic of the Fluidized Bed

It was found that the solid fraction measured using the bed height agreed with the value calculated from the manometer reading. This provided justification for the use of the manometer to obtain the solid fraction when measurement of the bed height was not possible because it had expanded beyond the working section. Typically particle collisions with the wall or hydrophone have a duration of the order of a few microseconds and it is therefore necessary to select a detector with a very high frequency response. The flush mounted hydrophone employed here has a frequency response of the order of 100 kHz. The active face of the hydrophone (about 3.5 mm in diameter) senses the particle collisions and produces a voltage output proportional to the magnitude of the impulse of the collision. This active area has a roughly uniform sensitivity except at the edges. The typical signal resulting from a collision of a single particle with the active face, consisted of positive spike of approximately 30 μsec duration followed by decaying oscillations which probably represent the dynamics of the hydrophone itself. This signal was high pass filtered and processed through a device which generates the envelope of the oscillatory spike from each collision. The output is fed into a HP 5326B timer counter which records the number of collisions per second above a threshold output voltage level set by the user. When the calibration is applied to this data it allows calculation of a cumulative collision impulse probability function $F(v^*)$, defined as the number of collisions per second above an impulse threshold level, v^*.

The hydrophone will also pick up noise due to particle-particle collisions, turbulence and particle-wall collisions away from the surface of the probe. To evaluate this noise the active face of the hydrophone was covered with a perforated disc thus preventing the measurement of direct collisions with the active face while recording the noise. It was observed that when the threshold voltage was set below a certain critical noise level the cumulative frequency recorded by the HP counter registered a sharp increase. This established the lower limit, v', at which it was appropriate to set the threshold. It also showed that a threshold level higher than this critical value, v' would record only collisions with the active face of the hydrophone.

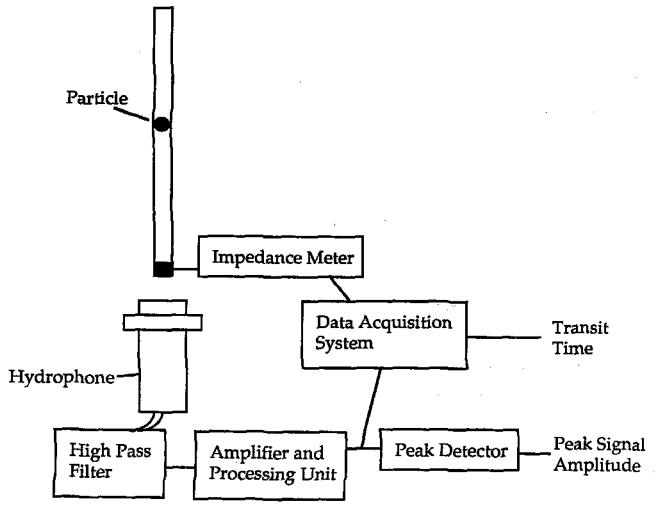

Figure 2: Schematic of the Hydrophone Calibration Device

The hydrophone was calibrated to evaluate the magnitude of the collision impulses and the apparatus used for the calibration is shown in Figure 2. It consisted of a glass tube with a copper band at the tip followed by the hydrophone. To simulate the actual conditions in the fluidized bed, this apparatus was placed under water. The copper band was used as part of an impedance meter and produced a voltage output whenever a particle passed through it. A voltage output pulse was also produced whenever the particle hit the hydrophone. A data acquisition system was used to obtain the time between the two pulses from which the incident velocity, u of the particle could be calculated. The rebound velocity was assumed to be negligible compared to the impact velocity. Then the magnitude of the impulse is defined as $I = mu$ where m is the measured mass of the particle. This was calibrated against the peak amplitude of the processed hydrophone output measured

using the peak detector. These calibrations were performed with both glass particles and lead shot and the results are included in Figure 3. One of the problems with the calibration method was that data could only be obtained for particle velocities close to the terminal velocity of the particle in water. Thus the data for the lead shot and the glass bead calibrations are clustered as shown in Figure 3. It is at least reassuring that both groups of points lie on roughly same straight line through the origin. The slope of this straight line, obtained by a linear least squares fit, was used as the calibration factor, k , for the hydrophone. Possible reasons for the scatter observed here are the differences in the way a particle hits the active surface and differences in deceleration as the particle approaches the active surface. Scatter could also result from differences in the particle mass due to non-uniformity in particle size.

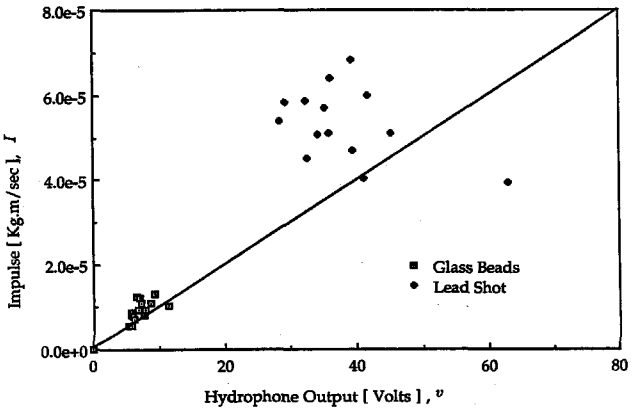

Figure 3: Hydrophone calibration showing the impulse plotted against processed peak output from the hydrophone and its signal conditioning unit.

4. Data Processing and Calculation

The data from a single experiment consisted of the collision number probability function, $F(v^*)$, where v^* is the threshold voltage level. Specifically $F(v^*)$ is the number of impulses per second for which the peak transducer output voltage is greater than v^* volts. Each impulse, I, has magnitude $I = kv$, where v is the peak voltage. It follows that if $\phi(v)dv$ denotes the number of collisions per second between impulse levels kv and $k(v + dv)$ then

$$F(v^*) = \int_{v^*}^{\infty} \phi(v)dv \tag{2}$$

Furthermore the force exerted on the active surface of the hydrophone, f is given by

$$f = \int_0^{\infty} kv\phi(v)dv \tag{3}$$

and

$$\phi(v) = -\frac{dF}{dv} \tag{4}$$

Hence, the granular pressure, P is given by

$$P = -\frac{k}{A}\int_0^{\infty} \frac{dF}{dv} vdv \tag{5}$$

where A is the active area of the hydrophone.

Integrating by parts and using the fact that $F(v) = 0$ above a finite value of v (since impulses of infinite magnitude are not possible), one obtains

$$P = \frac{k}{A}\int_0^{\infty} F(v)dv \tag{6}$$

Similarly the mean impact velocity, $\overline{u}$ is given by

$$\overline{u} = \int_0^{\infty} \frac{kv}{m}\phi(v)dv \Big/ \int_0^{\infty} \phi(v)dv = \frac{A}{mF(0)}P \tag{7}$$

and the mean square velocity, $\overline{u^2}$ is given by

$$\overline{u^2} = \int_0^{\infty} \frac{k^2v^2}{m^2}\phi(v)dv \Big/ \int_0^{\infty} \phi(v)dv = \frac{2k^2}{m^2F(0)}\int_0^{\infty} vF(v)dv \tag{8}$$

Equations 6, 7 and 8 were used to calculate the granular pressure and the mean and the rms velocities from the raw data, $F(v)$. Note that $F(0)$ is the maximum number of impulses per second at zero threshold voltage level. However, presence of noise at low threshold voltages level prevents direct measurement of $F(0)$. The value of $F(0)$ is taken to be same as the the value of $F(v')$, where v' is the maximum amplitude of the noise measured when the face of the hydrophone was masked.

5. Experimental Results

The terminal velocities, u_∞, of the individual particles used in the fluidized beds were measured in a 109 cm length of 10.2 cm diameter tube. These values which agree well with previous measurements (for example that presented in Figure 8.1 of Wallis [1969].) are presented in Table 1 along with the corresponding Reynolds numbers, Re, based on u_∞ and particle diameter. These Reynolds numbers are appropriate parameters characterizing each of the four fluidized beds.

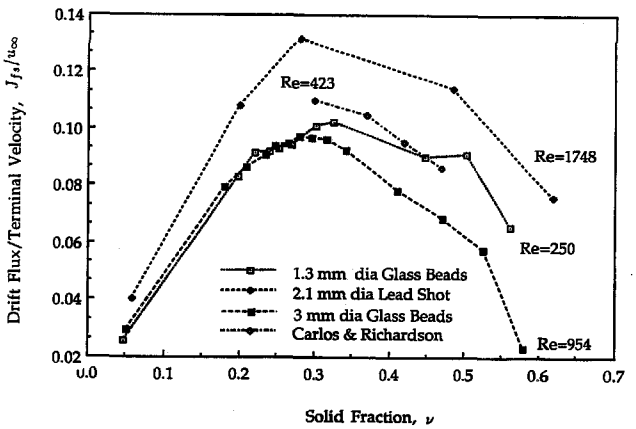

Figure 4: Dimensionless driftflux, J_{fs}/u_∞, as a function of solid fraction, ν, for the present experiment and those of Carlos and Richardson (1968).

In a fluidized bed the drift flux, J_{fs}, is defined by $J_{fs} = \nu(1-\nu)u_f$. The present flow rate data was converted to drift flux values which are presented nondimensionally in Figure 4.

This data is in good agreement with previous measurements, for example that obtained by Wilhelm and Kwauk [1948].

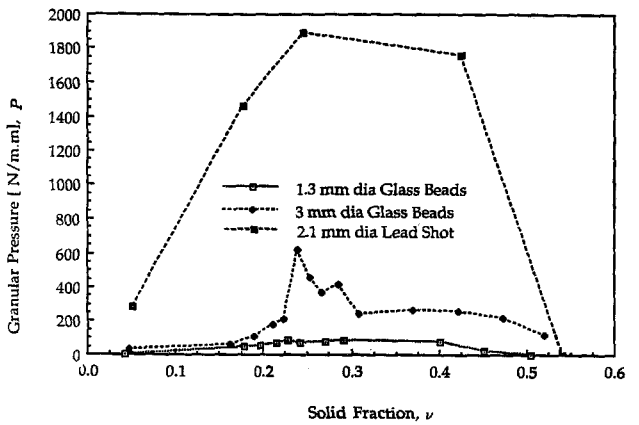

Figure 5: Granular pressure, P, as a function of solid fraction, ν, for the three fluidized beds.

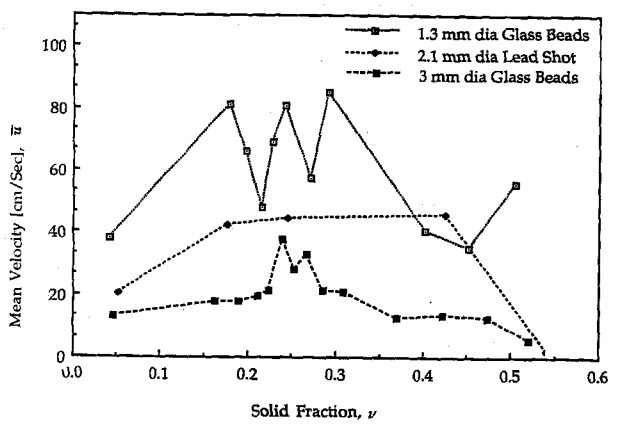

Figure 6: Mean impact velocity, $\overline{u}$, as a function of the solid fraction, ν, for the three fluidized beds.

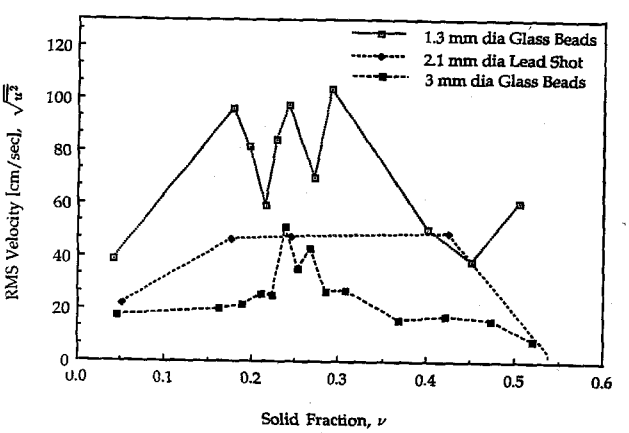

Figure 7: Mean rms velocity, $\sqrt{\overline{u^2}}$, as a function of the solid fraction, ν, for the three fluidized beds.

Granular pressure, mean velocity and rms velocity for the glass beads and the lead shot are plotted as functions of solid fraction in Figures 5, 6 and 7, respectively. By comparison the plastic particles yielded signals which were very much smaller and could not be distinguished from the background noise. Consider first the granular pressures. From a low value at high solid fractions the granular pressure increases as the solid fraction is reduced until it reaches a maximum; thereafter it decreases as the bed becomes quite dilute. The mean and rms velocities exhibit similar trends.

The kinetic energy of the particles in the bed may thought of as consisting of two components – transverse and longitudinal. These are due to transverse and longitudinal components of particle velocity. The granular pressure is a measure of the transverse kinetic energy of the particles. The number of collisions in a given time, between particles, approximately determines the conversion of the longitudinal kinetic energy into the transverse kinetic energy. The longitudinal kinetic energy of the particles is proportional to the fluid velocity in the bed. However, the number of collisions among particles in a given time is directly proportional to the solid fraction or inversely proportional to fluid velocity in the bed. Thus, the transverse kinetic energy has a maximum value as a result of the competing influence of these two factors. Hence, both the granular pressure and the velocities exhibit a maximum as the fluid velocity in the bed is increased.

It can be seen from Figure 5 that the lead shot exerts a much higher granular pressure than the glass beads and that the 3 mm glass beads exert a higher granular pressure than the 1.3 mm glass beads. The maximum values of the granular pressure are 1900, 630 and 100 pascals for lead shot, 3 mm glass beads and 1.3 mm glass beads respectively. The mean and rms impact velocities exhibit very similar trends. As shown in Figures 6 and 7, the 1.3 mm glass beads have higher impact velocities than the 3 mm glass beads while the lead shot has an intermediate level of impact velocity.

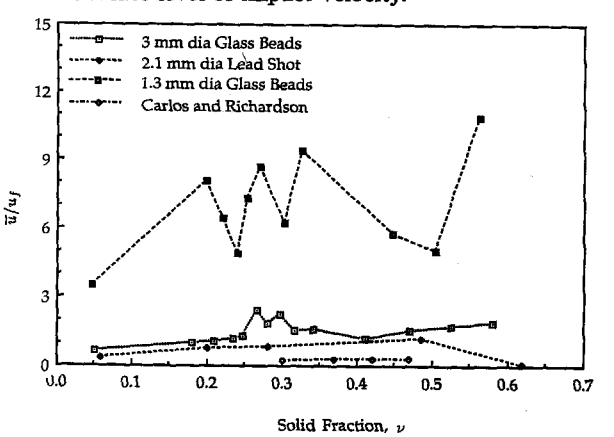

Figure 8: Ratio of the mean impact velocity to the mean fluid velocity, $\overline{u}/u_f$, as a function of solid fraction, ν, for the three fluidized beds and from the data of Carlos and Richardson (1968).

The results of Figures 5, 6 and 7 should also be presented nondimensionally in order to help understand the origins of these nonsteady effects. The most obvious nondimensional result is the ratio of mean granular velocity to mean fluid velocity, $\overline{u}/u_f$ and this is presented in Figure 8. It is readily observed that the values of this ratio are very different for the three

types of particles. On the other hand, $(\overline{u}/u_f)Re$ is similar for the three types of particles as can be seen from the Figure 9, where this quantity is plotted against ν.

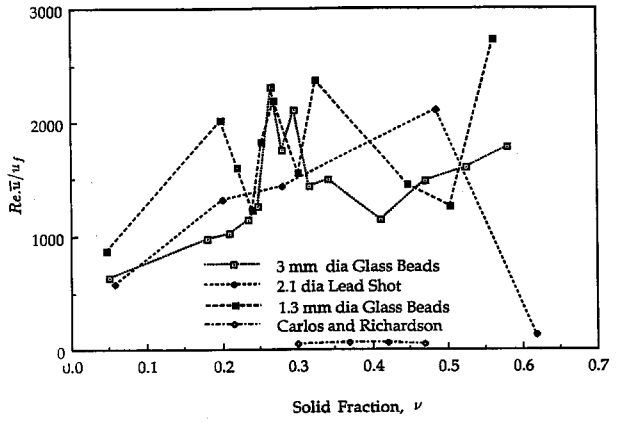

Figure 9: Product of the ratio of mean impact velocity to mean fluid velocity and the Reynolds number, $\rho_f u_\infty d/\mu_f$, as a function of solid fraction, ν, for the three fluidized beds and from the data of Carlos and Richardson (1968).

In a recent paper Lun and Savage (1988) attempted to extract information on the granular pressures and velocities from the experimental measurements of Carlos and Richardson (1968) who conducted an investigation on the unsteady velocities in fluidized beds consisting of 0.88 cm glass beads in the fluid Dimethyl Phthalate. The terminal velocity, u_∞ and Reynolds number, Re, of individual beads in this bed were about 40 and 423 respectively. Thus the experiments of Carlos and Richardson were somewhat similar to conditions in the present investigation except for the fact that that the particles were substantially larger and the beds were much shallower. These factors may be responsible for the observation that the unsteady velocities observed by Carlos and Richardson and used by Lun and Savage are very much smaller than the present data (as is shown graphically in Figure 8). But there are other possible reasons for the discrepancy. Carlos and Richardson (1968) used a movie camera with maximum framing rate of 64 frames/sec to record the unsteady motions. This rate would be sufficient to capture the large vortical motions inherent in such fluidized beds(see for example Kytomaa and Brennen(1986)). It would not however be adequate to detect the much higher frequency and smaller scale particle motions which are properly considered to constitute the granular temperature.

Acknowledgements

The authors are grateful to Steven Cecio and Professors Rolf Sabersky, Stuart Savage and Charles Campbell for helpful discussions and suggestions. We would also like to acknowledge the support of Union Carbide who have generously supported research in fluidized beds and granular material flows.

References

Carlos C.R. and Richardson J.F. (1968). *Solids Movement in Liquid fluidized Beds – I. Particle Velocity Distribution*, Chemical Engineering Science, Vol. 23, 1968, pp 813-824.

Lun C.K.K. and Savage, S.B. (1988). *Kinetic Theory for Rapid Flow of Dense Fluid–Solid Suspensions.* Submitted for publication in J. Fluid Mechanics.

Wallis G.B. (1969). *One-dimensional Two-phase Flow*, p93, 177.

Wilhelm, R.H., and Kwauk, M. (1948). *Fluidization of Solid Particles*, Chemical Engineering Progress, Vol. 44, pp 201-217, 1948.

Kytomaa, H.K. and Brennen, C.E. (1986). *Some Observations of Flow Patterns and Statistical Properties of Three Component Flows*, J. Fluids Engg., Vol. 110, No. 1, pp 76-84.